Modeling of nonlocal electron kinetics in a low-pressure inductively coupled plasma

V.I. Kolobov,[1,*] G.J. Parker,[2] and W.N.G. Hitchon[1]

[1] *Engineering Research Center for Plasma-Aided Manufacturing, University of Wisconsin–Madison, Madison, Wisconsin 53706*

[2] *Lawrence Livermore National Laboratory, 7000 East Avenue, L-418, Livermore, California 94550*

(Received 25 May 1995)

Two different kinetic calculations have been employed to model electron behavior in a low-pressure inductively coupled plasma (ICP) in order to investigate the processes governing the formation of the electron distribution function (EDF). One approach involves a numerical "propagator" treatment of time-resolved electron motion in five-dimensional phase space (two spatial and three velocity coordinates) based on the "convected scheme" (CS). The other one, referred to as the "nonlocal" approach, uses the difference between momentum and energy relaxation rates of electrons to simplify the Boltzmann equation. For the majority of electrons, the nonlocal approach reduces the kinetic equation for the isotropic part of the EDF to a form that exhibits a resemblance to that for homogeneous plasmas. Both calculations incorporate the principal physical effects in a collisional ICP: electron heating by an inductive electric field and nonlocal electron kinetics in which the electrons rapidly lose momentum but travel long distances before suffering a substantial energy loss in collisions. The collision processes that are important in the discharge include quasielastic and inelastic collisions with heavy particles and electron-electron interactions. A comparison of the results of the two methods validates the assumptions employed in the nonlocal approach for the considered range of discharge conditions. To good accuracy the EDF of the majority of the electrons in the ICP is found to be solely a function of the total (kinetic plus potential) electron energy and to be largely independent of the spatial coordinates. The extent to which this is true, and the circumstances under which it is true, are a major focus of this paper. In a rare gas ICP, as a result of Coulomb collisions between electrons, a Maxwell-Boltzmann distribution is typically found in the elastic energy range. The CS calculations demonstrate that trapped electrons can carry a substantial circulating current within the plasma that exceeds the current of free electrons to the walls.

PACS number(s): 52.80.−s, 52.65.−y

I. INTRODUCTION

A considerable interest in low-temperature plasmas has recently been generated by numerous modern applications to materials processing. Novel "high-efficiency" plasma sources have been introduced which are sustained by alternating electromagnetic fields at relatively low gas pressures of 1–100 mTorr and ionization degrees up to 10^{-2} [1]. Discharge modeling is important for understanding physical processes in the plasma and in source design. An accurate simulation requires, among other things, a precise knowledge of the electron distribution function (EDF) which defines the rates of plasma generation and various chemical reactions. These rates are not constant in space or time, nor simply related to the local fields or mean electron energy. Thus any model which hopes to do better than describe the qualitative behavior of the plasma must contain a rigorous kinetic treatment of the electron gas.

In the gas-discharge community attempts are still made to obtain the principal qualitative features of gas discharges within the fluid approach; kinetic analysis is used in this case only to calculate the values of transport coefficients and the rates of plasma chemical reactions. However, numerous nonlocal effects have been observed [2] which cannot be even qualitatively described by the fluid approach. Numerical gas-discharge modeling has evolved to include development of hybrid (fluid-particle) Monte Carlo models [3]. Statistical or particle-in-cell (PIC)–Monte Carlo methods have been introduced to gas-discharge physics from collisionless fusion plasmas and astrophysics [4]. A nonstatistical, propagator treatment of particle kinetics (the so-called convected scheme) demonstrated advantages compared to statistical methods [5]. Some of the numerical methods have been developed into reliable computer codes, capable of detailed simulations of the discharge plasma. However, they are often time consuming especially when applied to multidimensional plasma sources. Efficient numerical tools for the kinetic treatment of electrons and reliable approximate approaches to the solution of the Boltzmann equation are necessary.

In this paper we compare the results of two different kinetic calculations in application to inductively coupled plasmas (ICP's). One is a numerical "propagator" treatment of time-resolved electron motion in five-dimensional phase space (two spatial and three velocity coordinates) using the convected scheme (CS) [5–8]. Another, referred to as a "nonlocal approach" [2,9–12] assumes small anisotropy of the electron distribution function (EDF) and uses the total energy of electrons as an independent

*Present address: Dept. of Chemical Engineering, University of Houston, Houston, TX 77204.

variable in the spatially inhomogeneous Boltzmann equation. Both these methods have already been used in different gas-discharge problems. This is the first paper to our knowledge where the CS was applied to description of electron kinetics in a two-dimensional plasma. The goal of the paper is to investigate the physical processes governing the electron behavior in a collisional ICP and the approximations which can be used to simplify the treatment of nonlocal electron kinetics at low gas pressures.

Self-consistent kinetic modeling of a two-dimensional ICP is a formidable numerical task. Though attempts have recently been published to this end [10,12,13], in our present study we consider the electron kinetics for given distributions of electrostatic and alternating electric fields. The calculations are, therefore, not fully self-consistent. The essential ICP physics incorporated in the models includes spatially inhomogeneous electron heating by the inductive electric field and various collision processes. Discharge conditions are such that the electrons rapidly lose *momentum* but diffuse throughout the whole discharge volume before suffering a substantial *energy* loss due to collisions. The nonlocal approach has proved to be insightful, yet computationally very efficient in application to different gas-discharge problems under these conditions [2]. The validity of the approximations employed in this approach, involving assumptions of small anisotropy and time independence of the principal part of the EDF, as well as the appropriateness of spatial averaging of the Boltzmann equation for calculation of the trapped-electron DF in an ICP, are examined using the CS. It is found that the EDF is largely independent of position. The extent to which this is true, and the circumstances under which it is true, are a major focus of this paper.

The ICP is a weakly ionized (the ionization degree is about 10^{-3}), bounded, electrodeless plasma sustained by an inductive electric field which results in electron heating. The plasma is created by electron impact ionization. The effective loss rate of electrons and ions is determined by their escape to the walls. The inductive electric field in the ICP is intrinsically nonuniform even in the absence of plasma shielding. The alternating electron current is closed within the plasma volume and does not form an oscillating rf sheath as in capacitively coupled plasmas. The plasma density in an ICP is typically higher than that in a capacitively coupled plasma. The thickness of the space charge sheath near the wall is negligible compared to the chamber dimensions. The majority of the electrons are trapped in the plasma by the electrostatic field which is established to equalize the electron and ion dc fluxes. The mechanism of electron heating in the ICP is a subject of intense research. At very low gas pressures, in a regime with rare collisions, collisionless heating of electrons may prevail over collisional (Ohmic) heating [14–16]. The present paper deals with the pressure range where collisional heating dominates. Even under these conditions some collisionless features of the electron behavior have been found in the CS calculations: for instance, a substantial circulating current exists within the plasma. Though the ionization degree is relatively low, the Coulomb collisions among electrons are shown to be important in maintaining the EDF and the ionization rate in a rare gas ICP.

In the next section we describe the formulation of the problem, with emphasis on the analytic technique. The nonlocal approach allows the problem to be cast in a form such that results for electron kinetics in a homogeneous plasma may be applied to the highly inhomogeneous ICP. The CS was described in detail elsewhere; some aspects of the CS used here are summarized in the Appendix. Section III presents the results of the calculations.

II. FORMULATION OF THE PROBLEM

We consider a weakly ionized low-pressure ICP sustained by an inductive electric field from a planar coil. The electrons and ions created by electron impact tend to diffuse out of the plasma, and, since electrons are faster, a slight positive space charge develops in the volume. The potential of the space charge field forms a potential well which traps the majority of the electrons in the plasma to assure the balance of the ionization rate and the loss rate. For the considered range of discharge conditions, the motion of the electrons in such a potential well is collision dominated. For ionization degrees typical of ICP's, electron collisions with neutrals are typically more frequent than collisions between the charged particles. Collisions with neutrals can be unambiguously divided into quasielastic and essentially inelastic by comparing the energy lost in a single collision with the energy scale of the EDF decay, $\Delta\varepsilon = [\partial \ln(F)/\partial w]^{-1}$ [2]. In quasielastic collisions (which include elastic collisions and excitation of molecular vibrations and rotations) the electron momentum undergoes a substantial change, while the relative change of the electron kinetic energy w is small compared to $\Delta\varepsilon$. The energy loss can be described by a parameter $\delta \ll 1$ which is the average fraction of energy lost in a single collision. Essentially inelastic collisions include those with an energy loss substantially greater than $\Delta\varepsilon$ (excitation of electron levels and ionization). For most gases, the total frequency of inelastic collisions, ν^*, is less than the momentum transfer frequency ν. Thus an electron undergoes many elastic collisions before an inelastic collision occurs. As a result, the electron energy relaxation length may exceed the discharge dimensions even if the electron mean free path for momentum transfer is small compared to those.

In our present study of the electron kinetics in the ICP, imposed spatial profiles of the electrostatic potential $\varphi(\rho, z)$ and the azimuthal component of the inductive rf electric fields, $E_\theta(\rho, z)$, are used. The spatial profile of $E_\theta(\rho, z)$ was obtained as a solution of the Maxwell equations for a given plasma density, and is shown in Fig. 1. The electrostatic potential is assumed to be of the form

$$\varphi(z,\rho) = \varphi_0 \left\{ 1 - \left[1 - \left(\frac{2z}{L} - 1 \right)^{\kappa_1} \right] \times \left[1 - \left(\frac{\rho}{R} \right)^{\kappa_2} \right] \right\}. \quad (1)$$

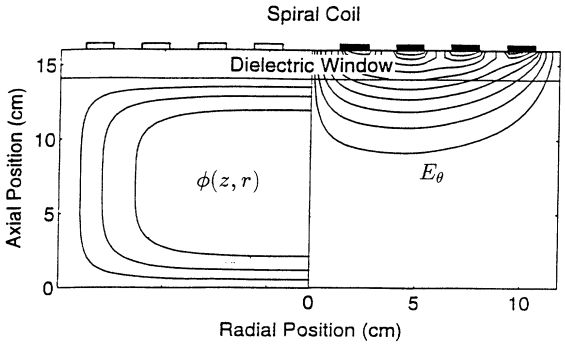

FIG. 1. The profile of the electrostatic potential and the azimuthal component of the rf inductive field E_θ used in simulations.

We varied κ_1 and κ_2 to examine the influence of the potential profile on the EDF shape. The wall potential φ_0 with respect to the peak plasma potential (taken to be zero) is set up to ensure the ionization balance. The procedure for calculation of φ_0 in the two methods is described below; $e\varphi_0$ must in any case exceed the first excitation level of the atoms ε^*.

The two methods of handling the Boltzmann equation will now be briefly reviewed.

A. Convected scheme

The convected scheme calculates the time-resolved particle density in the phase space. It employs a propagator to update the particle numbers in numerical "cells." This propagator is designed to satisfy Liouville's theorem and to exactly locally in phase space conserve such quantities as particle density, energy or momentum, and angular momentum in the numerical implementation of the particle kinetics. The CS distribution extends throughout the entire phase space, with essentially the same amount of information obtained for each numerical cell. As a result the CS method is unlike the Monte Carlo method which follows discrete particles and exhibits statistical "noise" which is problematic in the regions where the particle density (in phase space) is low. For many cells of the phase space mesh the expected number of Monte Carlo simulation particles in the cell will actually be much less than 1. The use of "weighting schemes" to mitigate this problem ultimately leads to algorithms such as the CS or EPIC [17], which are based on the method of characteristics. Eastwood [17] formally wrote a general representation of 1D methods of characteristics. When implemented numerically, unlike the CS he (i) used discrete particles, evaluating overlap integrals by sampling at the particle positions; (ii) recommended the particles be uniformly spaced at the new time level; and (iii) suggested that in more than 1D the variables be treated as separate. By contrast, in the CS we compute where the initial cell goes using conservation laws locally in phase space, and using the positions of the cell's spatial faces which stay in contact with their neighbors. The CS can be regarded as a method of characteristics with various desirable properties. The sheath regions and the tail of the distribution are well resolved by the CS. Elimination of various sources of numerical errors and implementation of the CS for different geometries were discussed previously [5–8].

The convected scheme used here provides an EDF as a function of six independent variables $(\rho, z, v_z, v_\perp, \mathcal{M}, t)$. Here (ρ, z) are cylindrical coordinates, v_z is the z component of velocity, $v_\perp$ is the magnitude of the component of velocity perpendicular to z, $\mathcal{M} = \rho \sin\phi_v$ is the "reduced" angular momentum or moment arm about the z axis, where ϕ_v is the angle between the velocity $v_\perp$ and the unit radial vector $\hat{\rho}$, measured clockwise with $\phi_v = 0$ being radially outward, and t is time. If the actual angular momentum about the z axis is $\mathcal{L}_z$, then $\mathcal{M} = \mathcal{L}_z/(mv_\perp)$, where m is the particle mass. In previous work, calculations were described using the variable sets $(z, v_z, v_\perp)$ [6,7] and $(\rho, v_z, v_\perp, \mathcal{M})$ [8] as well as (z, v, μ) [18] where v is the total speed and $\mu = v_z/v$. This is the first convected scheme calculation using the full set of variables $(\rho, z, v_z, v_\perp, \mathcal{M})$, although the extensions to previous work are straightforward. Some modifications to allow for the inductive electric field and minor changes in the collision operator are described in the Appendix. The parameters of the computational "mesh" used in the CS in the present work are given in Table I. The mesh is somewhat coarse with respect to the two spatial coordinates, while the mesh in $(v_z, v_\perp)$ is very fine. The number of $\mathcal{M}$ cells at each radius ρ depends on ρ and is equal to $4i$, where i is the ρ index, so the total number of $\mathcal{M}$ cells is $\sum_{i=1}^{N_\rho} 4i = 2N_\rho(N_\rho + 1)$ where N_ρ is the number of ρ cells.

The EDF $f(\rho, z, v_\perp, v_z, \mathcal{M}, t)$ is defined to be the number of particles in a particular cell at time t divided by the appropriate volume of the cell in phase space $2\pi\rho d\rho dz v_\perp dv_\perp dv_z d\phi_v$ where $d\phi_v$ is related to $d\mathcal{M}$. The isotropic or spherically symmetric part of the EDF $F_0(\rho, z, v, t)$ is constructed as an average over angles in the velocity space, i.e., over $\mathcal{M}$ (or ϕ_v) and over μ. The nonspherical component $F_1(\rho, z, \mathbf{v}, t)$ is therefore given by $F_1(\rho, z, \mathbf{v}, t) = F - F_0(\rho, z, v, t)$. The time-averaged part of F_0 can be constructed using a sum over the time steps in a rf cycle divided by the number of time steps

TABLE I. Parameters for CS simulation.

Quantity	Value
number of z cells	14
number of ρ cells	11
number of v_z cells	71
number of $v_\perp$ cells	36
number of $\mathcal{M}$ cells	528
total number of cells	9195494
max $(\frac{1}{2}mv_z^2)$	80 eV
κ_1	4
κ_2	4
max (n)	2×10^{11} cm^{-3}
power deposited	100 W
gas pressure	20 mTorr
gas temperature	300 K

per cycle.

For the CS calculations the peak electron density and the profiles of the rf inductive field $E_\theta(\rho,z)$ and electrostatic potential $\varphi(\rho,z)$ were specified externally in this non-self-consistent case. Both $E_\theta(\rho,z)$ and $\varphi(\rho,z)$ were scaled by an initial guess. As the simulation progressed, $\varphi(\rho,z)$ was rescaled (that is, φ_0 was varied) so that ionization and electron wall loss balanced. Once $\varphi(\rho,z)$ was found, E_θ was rescaled so that the power deposited into the plasma reached the desired value. The run was then restarted and iterated until the desired power deposition was obtained, the peak electron density was the specified peak density, and ionization was balanced by electron wall losses. In previous work using the CS in simpler discharges, the calculations were fully self-consistent and so the plasma density and all electric fields were calculated by the CS.

B. Nonlocal approach

The other method used here, which is referred to as a nonlocal approach, has also been described in detail in earlier work [2,9–12]. It uses the total electron energy as an independent variable in the spatially inhomogeneous Boltzmann equation in the two-term approximation. For the majority of trapped electrons in an ICP the Boltzmann equation is reduced to only one variable (total energy). This simplification, which is primarily attractive for multidimensional plasmas, provides a useful link to electron kinetics in a homogeneous plasma. It enables one to use the results of studies of the local Boltzmann equation, in particular in regard to the way the collision cross sections control the shape of the EDF in a rf plasma. A simplified model of electron kinetics such as is provided by the nonlocal approach is essential in order to interpret the results of the "exact" CS calculation. We shall discuss the extent to which the assumptions employed in the nonlocal approach are validated by the CS. The equations used in the nonlocal approach are the subject of the rest of this section.

The key assumptions in this part of the work are (i) the EDF is almost isotropic; the two-term approximation is applicable in the collisional regime when the electron mean free path for momentum transfer is much less than the discharge dimensions; (ii) the isotropic part of the EDF is nearly time independent; (iii) the total energy of electrons ε (kinetic plus potential) is an appropriate independent variable for use in the calculations; the principal part of the EDF for slow trapped electrons is a function *solely* of ε and does not depend explicitly on the coordinates.

These assumptions are based on the difference between the rates of momentum and energy relaxation of electrons. The collision processes which are important for the ICP include electron collisions with heavy particles and Coulomb interactions among charged particles. For the majority of electrons in an ICP, the momentum relaxation is governed primarily by elastic collisions with heavy particles. In elastic collisions, the electron momentum undergoes a substantial change, but not the electron energy. In Coulomb collisions, both the energy and the momentum of the electrons are changed only slightly. The fractions of electron energy and momentum lost in a collision with another electron are of the same order. The energy change is considerably smaller in collisions with ions and can be neglected. The smallness of the anisotropy of the EDF is a result of the difference between the rate of the momentum change in collisions and the rate of the energy change in any process.

The nonlocal approach makes use of the difference between the characteristic time scales for the evolution of the spherically symmetric (isotropic) and the nonspherical (anisotropic) parts of the EDF. The time evolution of the anisotropic part F_1 is governed by the transport frequency ν which describes the momentum relaxation rate. The time evolution of the isotropic part F_0 is relatively slow compared to the time evolution of F_1. It is characterized by an energy loss frequency $\nu_\varepsilon(v)$ which substantially depends on electron energy. For quasielastic collisions $\nu_\varepsilon = \delta\nu$. If the rf driving frequency $\omega \gg \nu_\varepsilon$, then the F_0 component is modulated only slightly with time. An average of the isotropic part F_0 over the rf period results in a steady component f_0. It can be seen that the correction $F_0 - f_0$ varies in time with a frequency 2ω, while the amplitude of the F_0 modulation is of the order of ν_ε/ω.

In deriving these conclusions we did not assume that the nonspherical component was small. The only important consideration was that the time scales are quite distinct: $\nu \gg \nu_\varepsilon$. The conclusion about the small modulation of the spherical component F_0 is therefore rather general and must be valid in the free-flight regime of ICP operation (rare collisions) as well. Since the spherical component defines the scalar characteristics of the electron ensemble, such as the electron density, these are practically time independent at $\omega \gg \nu_\varepsilon$. As a consequence of $\nu_\varepsilon \ll \nu$, the assumption (iii) above is expected to be valid also in the free-flight regime.

In the collisional regime, when the electron mean free path for momentum transfer $\lambda = v/\nu$ is small compared to the discharge dimensions, the traditional two-term spherical harmonic expansion for the EDF is applicable. The nonspherical part of the EDF, F_1, which is responsible for vector quantities such as electron fluxes, breaks into a steady-state part

$$\mathbf{F}_1^0 = -\lambda \nabla f_0 \tag{2}$$

and an oscillatory part

$$F_1^1 = \frac{eE_\theta(\rho,z)v_\perp}{\sqrt{\nu^2+\omega^2}} \frac{\partial f_0}{\partial \varepsilon} \cos(\omega t - \alpha) \sin\phi_v \tag{3}$$

which is proportional to the electric field strength E_θ [2]. Here $v_\perp$ is the magnitude of the velocity component in the plane orthogonal to the z axis, ϕ_v is the angle between the velocity $v_\perp$ and the radial vector which defines the particle position, and $\alpha = \arctan(\omega/\nu)$ is the phase of oscillations in F_1^1 with respect to the field oscillations. At $\omega \gg \nu$, the phase shift is $\alpha \sim \pi/2$, while in the opposite case the phase shift is small, $\alpha \ll 1$. Since the

field E_θ is directed along $\phi_v = \pi/2$ or $3\pi/2$, it does not affect the electrons moving outward ($\phi_v = 0$) or moving inward ($\phi_v = \pi$). To within an order of magnitude, the amplitude of the EDF modulation is proportional to the ratio of the directed azimuthal electron velocity to the characteristic thermal velocity of the electron motion. The expression (3) is valid if the amplitude of the EDF modulation is small compared to unity. It may not be applicable in the immediate vicinity of the coil where E_θ is high.

An equation for the time-averaged isotropic part of the EDF can be written in the form [2,11,12]

$$\nabla_r \cdot (vD_r \nabla_r f_0) + \frac{\partial}{\partial \varepsilon} v \left\{ (D_E + D_{ee}) \frac{\partial f_0}{\partial \varepsilon} + (V_{ee} + V_{eN}) f_0 \right\} = v\nu^*(v) f_0(\varepsilon) - vI. \quad (4)$$

The left hand side of Eq. (4) describes the electron diffusion in configuration space with the diffusion coefficient $D_r = v\lambda/3$ and electron motion along the "energy axis" due to energy loss (transfer) in collisions and heating. Both quasielastic collisions with neutrals and Coulomb interactions among electrons are written in the Fokker-Planck form in Eq. (4). Coulomb interactions result in electron diffusion along the energy axis with the diffusion coefficient D_{ee} and dynamic friction with "kinematic" velocity V_{ee} which are proportional to the electron-electron collision frequency ν_{ee} [11]. The energy loss in quasielastic collisions leads to dynamic friction with velocity $V_{eN} = w\delta\nu$ where δ is the average fraction of the energy lost in a single collision (for elastic collisions δ is a double ratio of electron to ion mass). The quantity D_E (defined below) is the energy diffusion coefficient due to the rf field. The right hand side of (4) describes inelastic collisions. Inelastic collisions are experienced by electrons with kinetic energy exceeding the inelastic threshold ε^*. An inelastic collision usually causes almost complete loss of the electron's energy. The specific form of the source term I in Eq. (4), which describes the arrival of electrons as a result of inelastic collisions and ionization, can be found elsewhere [2,11,12]. The electron heating by the rf field results in diffusive motion of electrons along the "energy axis" with diffusion coefficient [2,9–12]

$$D_E(\rho, z, \varepsilon) = \frac{[eE_\theta(\rho, z)\lambda]^2 \nu^3}{6(\nu^2 + \omega^2)}. \quad (5)$$

It should be noted that for collisional (Ohmic) heating the diffusion coefficient D_E is a function of the local rf field.

Equation (4) describes the energy relaxation of electrons due to collisions. In quasielastic collisions an electron loses a small fraction δ of its energy. Thus the energy relaxation length in quasielastic collisions, λ_T, is equal to the net electron displacement after $1/\delta$ collisions. Since the electron performs a random walk with the step size λ, the length λ_T is equal to $\lambda_T = \lambda/\sqrt{\delta}$. The EDF relaxation due to interelectron interactions occurs during the time ν_{ee}^{-1}. Thus the EDF relaxation length due to interelectron interactions, $\lambda_{ee} = \lambda\sqrt{\nu/\nu_{ee}}$, corresponds to a distance an electron travels during the time ν_{ee}^{-1}. Inelastic collisions of fast electrons occur during the time $1/\nu^*$. The net electron displacement during this time, $\lambda^* = \lambda\sqrt{\nu/\nu^*}$, corresponds to the energy relaxation length for inelastic collisions. Since the frequences ν_{ee} and ν^* as well as the quantity δ are functions of electron kinetic energy, the energy relaxation lengths are substantially different for electrons with different energies.

The numerical solution of Eq. (4) with appropriate ICP boundary conditions has been performed in Ref. [11] for trapped and free electrons with total energy of the order of and above the excitation threshold ε^*. The EDF of free electrons strongly depends on the coordinates. For trapped electrons with $\varepsilon \approx \varepsilon^*$, almost the entire discharge volume is available since the potential drop in the plasma is less than ε^*.

For the majority of electrons in the ICP, a further simplification of Eq. (4) is possible. Under nonlocal conditions, the spatial electron diffusion [described by the first term in Eq. (4)] occurs faster than electron displacement along the energy axis (described by other terms). For those electrons whose total energy does not exceed the depth of the potential well, $\varepsilon < e\varphi_0$, the time-average isotropic part of the EDF, f_0, can be expressed in the form [2]

$$f_0(\rho, z, \varepsilon) = f_0^0(\varepsilon) + f_0^1(\rho, z, \varepsilon) \quad (6)$$

where the main part $f_0^0(\varepsilon)$ is a solution of the appropriately spatially averaged Boltzmann equation, and $f_0^1(\rho, z, \varepsilon)$ is a small correction, $f_0^1 \ll f_0^0$. The EDF f_0^0 provides zero dc particle flux at each ε since the mobility and diffusion dc fluxes calculated from $f_0^0(\varepsilon)$ cancel each other at every ε. However, the *energy* fluxes calculated with f_0^0 are compensated only on average over the volume of the discharge. When $f_0^1(\rho, z, \varepsilon)$ is neglected, the dc flux of electrons is only due to those electrons (with $\varepsilon > e\varphi_0$) which are capable of escaping the discharge. The EDF of these free electrons depends explicitly on the coordinates [11]. The small correction term f_0^1 gives a nonzero dc flux of trapped electrons. Since electrons with different total energies diffuse almost independently, the net dc electron fluxes at different ε can flow in different and even in opposite directions, as illustrated below by the CS calculations. Such problems where different parts of the distribution behave quite differently from each other can evidently be handled only kinetically and cannot be obtained in the framework of a fluid treatment of the electron gas.

Under nonlocal conditions, the entire available discharge volume has a role in the formation of $f_0^0(\varepsilon)$. Since electrons have time to diffuse throughout the entire available discharge volume before they significantly change their total energy, the principal part of the EDF is defined by the spatially averaged equation [2,9–12]

$$\frac{d}{d\varepsilon} \left\{ (\langle vD_E \rangle + \langle vD_{ee} \rangle) \frac{df_0^0}{d\varepsilon} + (\langle vV_{ee} \rangle + \langle vV_{eN} \rangle) f_0^0 \right\} = \langle v\nu^*(v) \rangle f_0^0(\varepsilon) - \langle vI \rangle. \quad (7)$$

The angular brackets $\langle\,\rangle$ designate integration over the volume of the discharge accessible to electrons with given ε. For instance,

$$\langle vD_E\rangle = \frac{2\pi}{V(\varepsilon)}\int_{S(\varepsilon)} vD_E\rho d\rho dz, \tag{8}$$

where $S(\varepsilon)$ is the available discharge area bounded by the curve $\varepsilon = -e\phi(z,\rho)$ and $V(\varepsilon)$ is the available discharge volume.

According to Eq. (7), the shape of $f_0^0(\varepsilon)$ is governed by the integral balance of electron heating and energy loss (transfer) in various collisions. The effective heating rate is determined by the spatially averaged value of $D_E(\rho,z,\varepsilon)$ and thus depends on the spatial profiles of both the rf and electrostatic fields as well as on the functional dependence of the transport collision frequency ν on the electron speed.

Equation (7) coincides formally with the Boltzmann equation in a homogeneous plasma. However, all the necessary spatial information is contained in the coefficients in this equation and is retained in the nonlocal EDF $f_0^0(\varepsilon)$ [4,9–12]. A formal solution of Eq. (7) can be obtained considering D_{ee} and V_{ee} to be known functions. The solution in the elastic energy range which corresponds to zero electron flux along the energy axis is

$$f_0^0 = C\exp\left[-\int_0^\varepsilon \frac{d\varepsilon'}{\Delta\varepsilon(\varepsilon')}\right] \tag{9}$$

where

$$\Delta\varepsilon = \frac{\langle vD_E\rangle + \langle vD_{ee}\rangle}{\langle vV_{ee}\rangle + \langle vV_{eN}\rangle} \tag{10}$$

is the characteristic scale of the energy decay and C is a constant to be determined by imposing the normalization condition. The inelastic collisions lead to the appearance of an electron flux along the energy axis. Accounting for this flux results in an EDF which still has an important exponential part given by Eq. (9). If the Coulomb collisions are not very frequent, the EDF in the inelastic energy range decreases much more rapidly than f_0^0 in the elastic range, given in Eq. (9).

The total number of inelastic collisions and electron escapes to the walls per unit time can be expressed using the spatially averaged kinetic equation (7). Integrating (7) over ε from ε^* to infinity, one obtains in the black-wall approximation [2]

$$Q + Z = -\langle vD_E\rangle \left.\frac{df_0}{d\varepsilon}\right|_{\varepsilon^*}. \tag{11}$$

The first term Q in Eq. (11) is the total number of inelastic collisions, and the second Z is the total number of electron escapes to the walls. The latter, Z, can be expressed as the flux along the energy axis at $e\varphi_0$ [2]:

$$Z = -\langle vD_E\rangle \left.\frac{df_0}{d\varepsilon}\right|_{e\varphi_0}. \tag{12}$$

The ionization rate is in general the sum of the rates of direct ionization, stepwise ionization, and ionization in collisions of metastable atoms. The number of stepwise ionization events can be related to the total number of inelastic collisions, using an ionization efficiency coefficient $g < 1$ [2]. The total number of ionizations must be equal to the total number of electron escapes to the wall. Thus Eqs. (11) and (12) result in a relation between EDF derivatives at $e\varphi_0$ and ε^*:

$$\left(1+\frac{1}{g}\right)\left.\frac{df_0}{d\varepsilon}\right|_{e\varphi_0} = \left.\frac{df_0}{d\varepsilon}\right|_{\varepsilon^*}, \tag{13}$$

which defines the wall potential. The latter depends on the mechanism of ionization through the efficiency of stepwise ionization g. The quantity g can be expressed using the rate of stepwise ionization, the probability for the escape of resonance radiation, and the rates at which metastable atoms diffuse to the walls [2]. The wall potential was calculated from Eq. (13) for $g = 1/3$.

III. RESULTS FOR AN ICP IN A RARE GAS

In this section we present the results obtained by the two methods for an ICP in a rare gas. To examine the role of different collision processes on the EDF shape, we consider both argon and helium at a pressure of $p = 20$ mTorr. The discharge is sustained by an inductive rf field of frequency $\omega = 85\times10^6$ s^{-1} (13.56 MHz) from a planar coil placed on a dielectric window on top of a cylindrical chamber of radius $R = 12$ cm and height $L = 14$ cm. The azimuthal component of the inductive electric field E_θ is obtained as a solution of the Maxwell equations for given coil current and plasma density, assuming the walls and bottom of the chamber are metallic [10–12]. The spatial profile of E_θ is shown in Fig. 1 together with the shape of the electrostatic potential φ. The influence of the rf magnetic field on electron kinetics is neglected since it is not believed to be important for the collisional (Ohmic) electron heating examined here. The parameters of the collisional low-pressure ICP we consider in the present work correspond to the higher range of pressures in which ICP's are employed for material processing applications. The comparison of the results of the two methods allows one to gain insight into the physical processes governing the EDF formation in the discharge and examine the approximations which can be used to simplify the treatment of nonlocal electron kinetics in a low-pressure ICP.

A. Results of the nonlocal approach

The EDF in a low-pressure ICP was calculated using the nonlocal approach for different plasma densities. The approximations used for collision cross sections are shown in Table II. The CS uses a very detailed set of data described in Refs. [6–8]. Table III shows typical frequencies and lengths in argon and helium at pressure p =20 mTorr and for an ionization degree of 10^{-4}. It is seen that the momentum transfer frequency ν dominates over the total frequency of inelastic collisions ν^* and over the

TABLE II. Approximations for electron-atom collision frequencies used in the nonlocal approach: transport frequency $\nu = \nu_0 p(w/\varepsilon^*)^l$; total frequency of inelastic collisions $\nu^* = \nu_0^* p(w/\varepsilon^* - 1)$; fraction of energy loss in elastic collisions $\delta = 2m/M$.

Atom	ν_0 (10^9 s^{-1})	ν_0^* (10^9 s^{-1})	l	ε^* (eV)	$10^4\delta$
Ar	17	1.7	3/2	11.2	46
He	2.5	0.84	0	21.2	0.68

frequency of Coulomb interactions among electrons ν_{ee}. The energy relaxation lengths in different types of collisions correspond to net distances traveled during the time between subsequent collisions. The values of energy relaxation lengths in quasielastic collisions $\lambda_T = \lambda\delta^{-1/2}$, in interelectron interactions $\lambda_{ee} = \lambda(\nu/\nu_{ee})^{1/2}$, and in inelastic collisions $\lambda^* = \lambda(\nu/\nu^*)^{1/2}$ are given in Table III. It is seen that the energy relaxation lengths exceed the discharge dimensions, i.e., the assumptions employed in the nonlocal approach are appropriate for the considered range of discharge conditions.

We first consider the EDF formation in the absence of electron-electron interactions. In this case, the EDF shape is governed by the energy gain from the field and energy loss in collisions. For a rectangular potential well [$\kappa \gg 1$ in Eq. (1)], the spatial averaging (8) results in

$$\langle vD_E\rangle = \left(\frac{2}{m}\right)^{3/2} \frac{e^2\nu\varepsilon^{3/2}}{6(\nu^2+\omega^2)}\langle E_\theta^2(\rho,z)\rangle. \tag{14}$$

The electron heating is therefore governed by an effective field $E_{eff} = \sqrt{\langle E_\theta^2(\rho,z)\rangle}$. The characteristic length $\lambda_E = \varepsilon^*/eE_{eff}$ corresponds to the distance over which an electron would gain energy ε^* in a homogeneous electric field of strength E_{eff} in the absence of energy loss in elastic collisions [2]. For $\lambda_E \ll \lambda_T$, the energy loss in elastic collisions is negligible; the energy balance of electrons is governed by the field and the energy loss in inelastic collisions. In this case, the electrons gain energy in the elastic energy range $\varepsilon < \varepsilon$ [8] and lose their energy in the inelastic energy range $\varepsilon > \varepsilon$ [8]. The solution of (7) in the elastic energy range, which corresponds to constant electron flux along the energy axis, is

$$f_0^0 = C\int_\varepsilon^{\varepsilon_0} \frac{d\varepsilon}{\langle vD_E\rangle}, \tag{15}$$

where the upper limit ε_0 is defined by matching to the EDF tail. At $\lambda^* \ll \lambda_E$ the relative number of electrons in the inelastic energy range is small, and the upper limit in the integral (15) is $\varepsilon_0 \approx \varepsilon^*$. The shape of the EDF (15) is determined mainly by the functional dependence of the electron momentum transfer frequency on the electron energy. For an increasing function $\nu(v)$, the EDF has a concave curvature on a logarithmic plot versus energy and is enriched at both low and high energies compared to the Maxwellian distribution. The EDF may have a singularity at low energies due to two circumstances. First, the solution (15), which corresponds to conservation of the electron flux, diverges at low energies as $\varepsilon^{-1/2}$ for a constant diffusion coefficient D_E (as in helium). Second, if $\nu(\varepsilon)$ decreases with decreasing of energy (as in argon), the low-energy electrons absorb energy from a rf field less effectively than the high-energy electrons. They tend to accumulate at zero energy, which causes a strong peak at $\varepsilon = 0$. In the ICP, the joint effects of strong nonuniformity of the inductive electric field together with the presence of the ambipolar field additionally contribute to accumulation of electrons at low energies. The spatially averaged energy diffusion coefficient [Eq. (5)] vanishes at low energies for two reasons: (i) it is reduced by an additional factor because of the decrease in the area $S(\varepsilon)$ accessible to low-energy electrons, and (ii) being trapped by the ambipolar electric field, slow electrons (with small ε) cannot even reach the region of high inductive field where the heating takes place.

In the presence of Coulomb collisions (at higher plasma density) the low-energy electrons can interact with other electrons of higher energy and in so doing climb up in energy. The Coulomb interactions lead therefore to the heating of slow electrons and cooling of the fast electrons. They mitigate the accumulation of slow electrons near $\varepsilon = 0$ and can drastically reduce the peak of the EDF at $\varepsilon = 0$. Figure 2 illustrates the influence of interelectron collisions on the EDF shape in the energy range below the wall potential. The EDF's shown are obtained as numerical solutions of Eq. (7) for three different plasma densities with effective values of the inductive field E_{eff}=0.5 V/cm in argon and 2 V/cm in helium. It is seen that the Coulomb interactions result in significant changes of the EDF. A similar behavior has been found in a homogeneous rf plasma of rare gases at reduced gas pressures

TABLE III. Characteristic frequencies and lengths for electron kinetics in an ICP in argon and helium at a pressure p=20 mTorr and a plasma density $n = 10^{10}$ cm^{-3}. rf field frequency $\omega = 8.5 \times 10^7$ s^{-1}. Elastic and Coulomb collision frequencies are for an electron energy $w = 0.5\varepsilon^*$, and the inelastic frequency for $w = 1.2\varepsilon^*$.

Atom	ν (10^7 s^{-1})	ν^* (10^7 s^{-1})	$\delta\nu$ (10^4 s^{-1})	ν_{ee} (10^4 s^{-1})	λ (cm)	λ_T (cm)	λ_{ee} (cm)	λ^* (cm)
Ar	13	3.4	0.36	2.8	0.75	146	74	4
He	5	1.7	1.35	1.12	3.86	235	258	21

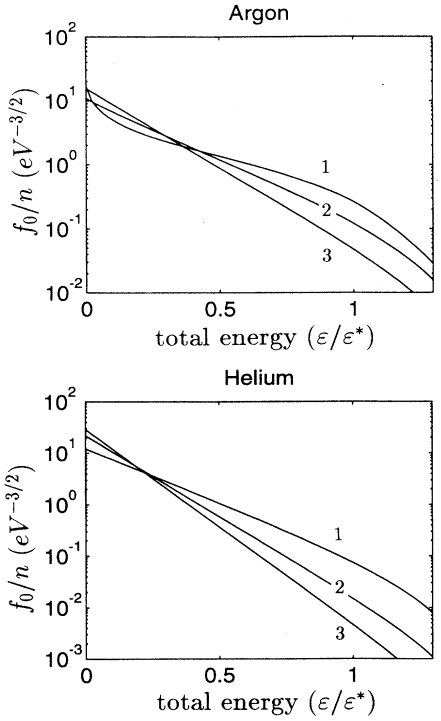

FIG. 2. The time-averaged isotropic part of the EDF f_0 in argon and helium found from the nonlocal model. The curves f_0/n are shown as functions of the total energy, at different plasma densities: $7\times10^8(1), 7\times10^9(2)$, and $5\times10^{10}(3)$ cm^{-3}.

[19].

The changes of the EDF induced by interelectron collisions have a significant influence on the electron characteristic energy $\Delta\varepsilon$, a key parameter that determines the profile of the ambipolar potential in the plasma. If the EDF is non-Maxwellian as a function of total energy, i.e., $\Delta\varepsilon$ depends on ε, the EDF as a function of kinetic energy changes with position and the mean energy of the electrons is spatially nonuniform [20]. In rare gases, at plasma parameters typical of an ICP, the EDF in the elastic energy range is found to be Maxwellian. The characteristic energy $\Delta\varepsilon$ does not depend on ε in this case, and the electron temperature $T_e = \Delta\varepsilon$ is spatially uniform. It should be emphasized that the temperature is determined by the integral balance of electron heating and cooling rather than local field values and thus influenced by the entire profiles of the rf field and the electrostatic field in the plasma.

B. Results of the CS simulation

Both Ar and He discharges were simulated using the CS. Table IV summarizes the results. Experimental results for an Ar discharge are also given for comparison. The wall potential and average energy obtained agree at the 10% level. In both simulations, the total power deposited into the plasma from the rf inductive field E_θ was

TABLE IV. Summary of CS simulation for Ar and He ICP discharges.

Quantity	He	Ar	Ar Expt.
φ_0 (V)	34	16.9	16.7
bulk $\langle\frac{1}{2}mv^2\rangle$ (eV)	7.3	4.2	3.9
max(E_θ) (V/cm)	4.8	4.24	

100±5 W and the final peak electron density $n \sim 2\times10^{11}$ cm^{-3}, which corresponds to the experimental discharge in Ar [21].

Figure 3 shows the EDF as a function of total energy plotted at different spatial positions within the volume of the discharge in Ar (a) and He (b). It is seen that to good accuracy the EDF's coincide with each other. The EDF is nearly Maxwellian in the elastic energy range and drops rapidly in the inelastic energy range due to inelastic collisions. Both results are in agreement with the nonlocal approach. The apparent disagreement for the EDF's at small and large z is the direct result of the

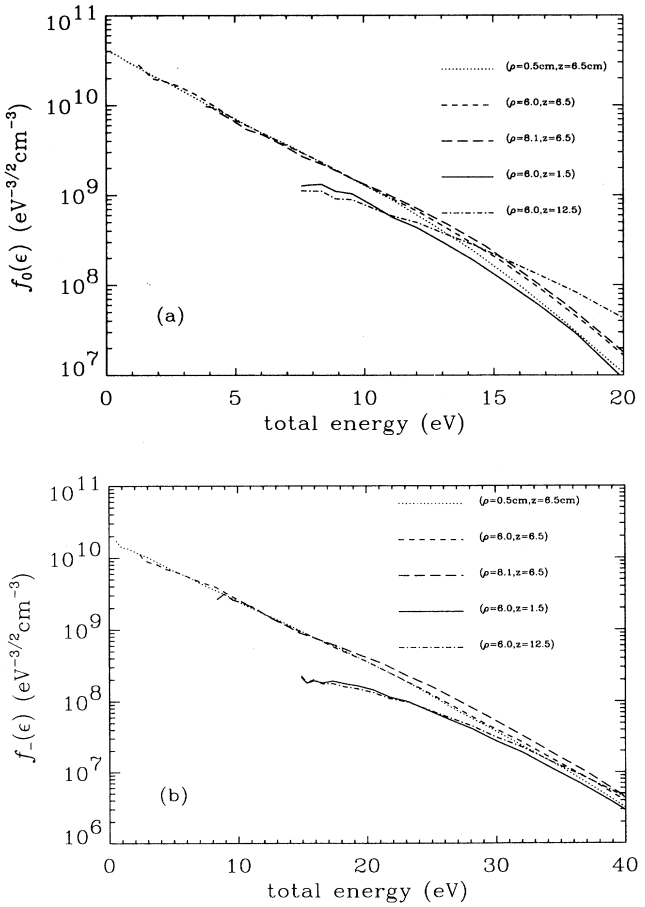

FIG. 3. The time-averaged isotropic part of the EDF f_0 in argon (a) and helium (b) as a function of the total energy, at different locations in the discharge, found from the CS.

coarse spatial grid used in the simulation. As the spatial mesh is refined, the electrostatic potential is better represented and therefore these EDF's tend to overlap the other EDF. However, the EDF near the coil does have an enhanced tail compared to the other EDF's due to the rf heating fields.

The EDF's as functions of kinetic energy at various times during the rf period are shown in Fig. 4 in the bulk of the Ar discharge (a) and in the vicinity of the coil (b). It is seen that the EDF is time modulated in the immediate vicinity of the coil, but not elsewhere.

Figure 5 illustrates the anisotropy of the EDF in an Ar discharge in the vicinity of the coil caused by the inductive electric field. It shows contour plots of $\log_{10} F(v_\perp, \phi_v)$ at different times for $v_z = 0$ from Eq. (3) (a) and CS simulation (b). Away from the coil, the EDF is nearly independent of ϕ_v. The field E_θ lies along $\phi_v = \pi/2$ or $3\pi/2$. During the first half cycle, E_θ is positive and electrons move towards $\phi_v = 3\pi/2$. The phase shift α depends on the electron energy in argon as is clearly seen from (a) at time $t = 0.375T$ where the phase changes its sign with increasing energy.

The total particle flux (integrated over the azimuthal angle in physical space) is shown in Fig. 6(a) for the Ar discharge. This flux is dominated by trapped electrons which represent the vast majority of the ensemble. The flux virtually vanishes near the walls and exhibits a circulatory pattern. The origin of the circulatory flux can be explained as follows. If the electron collision frequency with atoms vanishes at low energies in Ar, the slow electrons have virtually no collisions with atoms even at relatively high gas pressures. The inductive field E_θ gives the electrons near the coil (top and center of the plot) a high azimuthal velocity (in the direction normal to the page). In a collisionless regime, this causes a substantial centripetal force which pushes the electrons radially

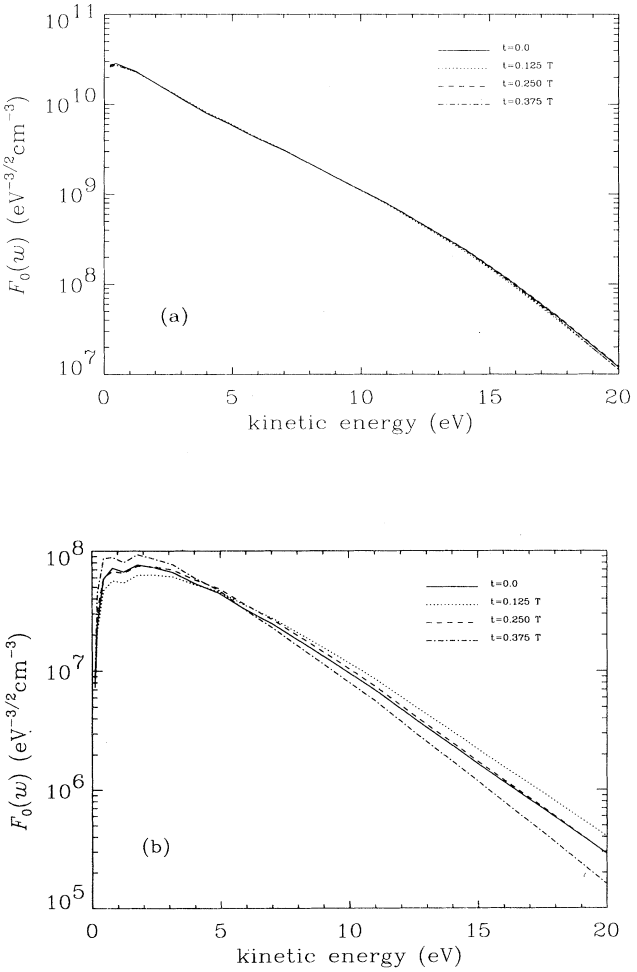

FIG. 4. The isotropic part of the EDF F_0 found from the CS in argon as a function of kinetic energy at two spatial positions for various times during the rf period (a) in the bulk $r = 0.4R, z = L/2$, and (b) close to the rf antenna $r = 0.4R$, $z = 0.96L$.

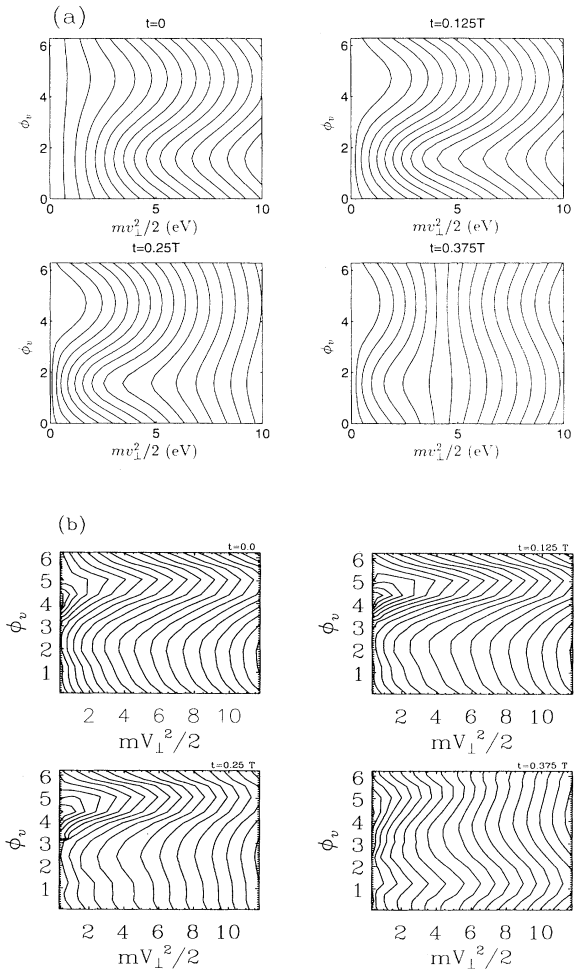

FIG. 5. Contour plots of $\log_{10} F(v_\perp, \phi_v)$ in the vicinity of the coil as functions of $mv_\perp^2/2$ and ϕ_v for $v_z = 0$ at different times (a) calculated from Eq. (3) at E_θ=2 V/cm and (b) CS simulations for $\rho = 0.4R$, $z = 0.96L$. Contours are at equally spaced intervals of $\log_{10} F$.

outward. When the electrons eventually do have collisions, which isotropize the EDF, the centripetal force is reduced. The centripetal force results in an outward flux of slow electrons in the vicinity of the coil. After collisions the electrostatic potential pushes the slow electrons radially inward again. For large z (near the top) this return flux is smaller than the outward flux of particles created by the coil, but near the bottom the inward flux is visible. Finally, the flux from the middle of the chamber at $z = L/2$ and $r = 0$ (on the left hand side of this plot) toward the coil (top and center) is driven by the density gradient since the maximum density is at $(r = 0, z = L/2)$.

Despite these fluxes being bigger than the flux of free electrons [see Fig. 6(b)], the trapped EDF is highly isotropic everywhere (Fig. 5). The very small anisotropy of trapped electrons leads to a noticeable flux because the density of slow electrons exceeds the density of fast electrons by orders of magnitude. However, free electrons

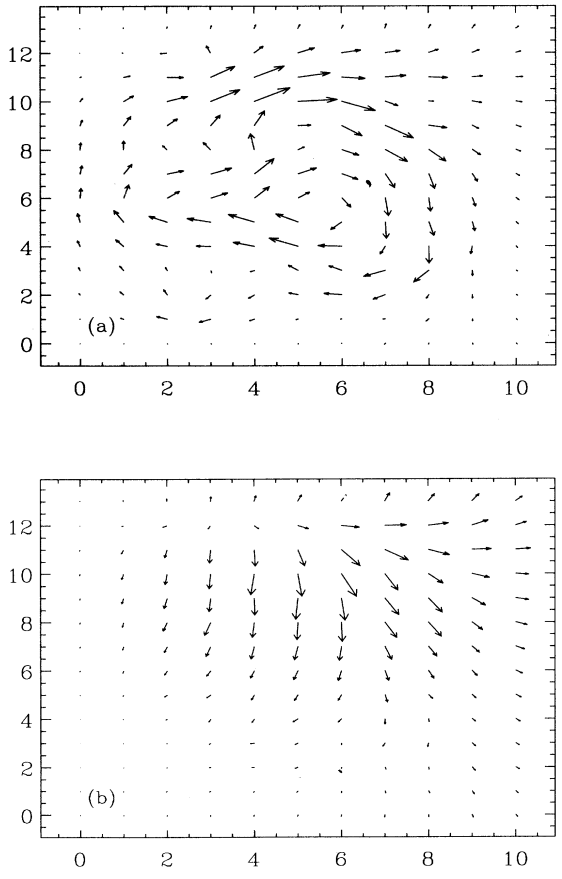

FIG. 6. The time-averaged electron fluxes in argon: (a) total, (b) free electrons. The components of the flux are the net numbers leaving per second through the corresponding faces of the cells of the mesh. The length of the vector is proportional to the flux; the longest vector corresponds to 3.2×10^{18} s^{-1} in (a) and 1.3×10^{18} s^{-1} in (b).

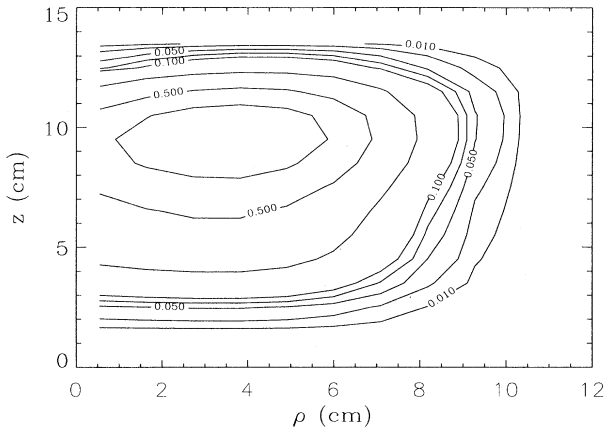

FIG. 7. The spatial profile of the direct ionization rate in argon. Contours are fractions of the peak ionization rate of 8.3×10^{15} cm^{-3} s^{-1}.

are the only electrons responsible for the electron flux to the walls. The circulatory flux is more pronounced in argon than in helium, due to the strong dependence of the electron collision cross section on electron energy in argon.

Figure 6(b) shows the flux of "free" electrons (electrons with $\varepsilon > e\varphi_0$). For these free electrons, there is no circulating pattern as found in the total electron flux. Instead, the flux is seen to come from the source region (see also Fig. 7) and escape to the walls of the discharge. A similar behavior of the free-electron flux has been obtained from the nonlocal approach [11].

The two-dimensional profile of the direct ionization rate is shown in Fig. 7. The peak of the ionization is observed off axis. In experiments [9] two peaks in the light emission have been observed in conditions similar to these. The origin of the central peak has been explained in [9,11] taking into account the radial nonuniformity of the static field. In our calculations the spatial profile of the static potential was rather flat; thus the contribution of trapped electrons to ionization is rather uniform. The off-axis peak is due to free electrons and occurs under the coil where they are heated most effectively. With a more radially nonuniform potential profile an on-axis peak may be obtained.

C. Discussion

The two calculations employed here both appear to provide an accurate description of electron kinetics in a low-pressure ICP in rare gases and to agree with each other in the considered range of discharge conditions. The extent to which the approximations employed in the non-local approach are valid, and the circumstances under which they are valid, have been the major focus of the present paper. The principal physical processes which govern electron kinetics in ICP in the discharge conditions considered involve the following:

(i) a spatially nonuniform collisional heating of electrons by the inductive field which is localized near the

coil;

(ii) the trapping of the majority of the electrons in the discharge volume by the electrostatic potential and the division of electrons into different groups which exhibit distinct behaviors;

(iii) the ionization degree being so high that Coulomb collisions can effectively transfer energy from the relatively energetic electrons, which are effectively heated by the rf inductive field, to the cooler electrons which cannot even visit the region where the heating occurs.

The division of electrons into different groups with respect to total energy is a rather common feature of electron kinetics in low-pressure gas discharges [2]. In the cathode region of a dc discharge, a division of thermal electrons into two groups results in a rather complex EDF [22]. The cathode plasma is characterized by a lower ionization degree than an ICP. The Coulomb collisions are less efficient here. Cold electrons trapped in the potential well typically have a Maxwell-Boltzmann EDF with temperature ~ 0.1 eV. The mean energy of free electrons is about equal to the excitation threshold energy. Since the densities of trapped and free electrons in the cathode plasma differ by orders of magnitude and change with the coordinates in an entirely different manner, the mean electron energy is spatially nonuniform [22,23]. Most of the electrons in the ICP are trapped in the plasma by the electrostatic field. For these electrons, the nonlocality condition is equivalent to a limit of high thermal conductivity. A hydrodynamic description of ICP electrons in this limit would give an erroneous result of uniform mean electron energy and uniform excitation (ionization) frequency over the plasma volume.

We have restricted our consideration to a collisional ICP, when the electron mean free path is much less than the discharge dimensions. At lower pressures the nonlocal method must be modified to include "collisionless" electron heating; the CS can be used essentially unchanged. The inductive electric field must be supplemented with the associated magnetic field and the entire Lorentz force used in the equation of electron motion Eq. (A2). The free-flight regime of ICP operation will be investigated elsewhere.

We have studied electron kinetics in an ICP composed of rare gases. In molecular gases, electrons mostly dissipate energy by exciting the vibrational and rotational energy levels of molecules. This case can also be described by Eq. (7) but the coefficient δ is not calculated as simply as for elastic losses, but is a function of electron energy. These losses are usually greater than elastic ones by one to two orders of magnitude; nevertheless, the corresponding coefficient is small ($\delta \sim 10^{-3} - 10^{-2}$). Thus the approximations employed in the nonlocal approach can be used in molecular gas plasmas as well but in a more limited range of discharge conditions. In a molecular gas ICP, the EDF is expected to be independent of the degree of ionization provided it is less than 10^{-4}.

IV. CONCLUSIONS

Two accurate kinetic treatments of electrons in two spatial dimensions were applied to a low-pressure collisional ICP. Some of the main results of the comparison of the two approaches for the considered range of discharge conditions include the following.

(a) The spherically symmetric (isotropic) part of the EDF, F_0, is time independent for the vast majority of electrons. Only a small modulation of the F_0 tail with a frequency 2ω was found from the CS simulation in the immediate vicinity of the coil. This result largely justifies the assumption in the nonlocal approach of a time-independent EDF.

(b) The nonspherical component of the EDF, F_1, is small with the sole exception of the coil vicinity where F_1 is modulated with the frequency ω and lags behind the inductive field. Again, the CS simulation agrees with the nonlocal assumption.

(c) The total electron energy is an appropriate variable for the analysis of the electron kinetics. For trapped electrons, the EDF's calculated by the CS and plotted as functions of total energy coincide at different spatial positions with good accuracy.

(d) In a rare gas ICP, the EDF shape is affected by interelectron interactions for an ionization degree as low as 10^{-8}. For a typical ICP ionization degree of 10^{-4} or greater, the energy transfer in Coulomb collisions results in a Maxwellian EDF in the elastic energy range. The electron temperature is spatially uniform and is determined by the integral balance of electron heating and cooling. The plasma density obeys the Boltzmann relation.

(e) The nonlocal approach transforms the problem of the EDF calculation in an ICP to a form similar to that in a homogeneous plasma. It makes possible use of the rich store of computational and experimental data for homogeneous rf plasmas to analyze the role of the various collisions in the formation of the EDF in an ICP.

(f) Substantial circulatory current was found in the CS simulation. The presence of this current within the plasma is attributed in part to "collisionless" behavior of the slowest electrons. The heating rate is slightly different in the two calculations due to the presence of noncollisional heating in the CS simulation.

In comparing the results of the two methods, one can see that for the operating parameters studied here the nonlocal approach works well as long as detailed behavior of the EDF near the coil is not considered. Furthermore, as the neutral pressure decreases, the two-term spherical harmonic expansion used in the nonlocal approach must be replaced by a more general expression. The "noncollisional" electron heating may become the dominant mechanism of heating in the regime with rare collisions. We believe that the magnetic force may influence the electron kinetics and the heating rate at low pressures and must therefore be included in both models.

ACKNOWLEDGMENTS

This work was supported in part by Intel Corporation and by the Engineering Research Center for Plasma-Aided Manufacturing, NSF Grant No. ECD-8721545.

APPENDIX

In this appendix, extensions of the convected scheme (CS) technique in two spatial and three velocity dimensions are discussed which are necessary for modeling electrons in an inductive electric field. We first describe the coordinate system and the mesh used for electrons in cylindrical geometry (Sec. 1). Section 2 treats the refinements of the "ballistic" and "collisional" propagators. Section 3 discusses the algorithm of the CS.

1. Coordinate system and mesh for electrons in cylindrical geometry

The coordinate system used to describe electron motion in this work is $(\rho, z, v_z, v_\perp, \mathcal{M})$, which is the same as in Refs. [6–8]. Here, z is the vertical distance from the chamber bottom, ρ is the radial distance from the center of the discharge, v_z is the velocity parallel to the z axis, $v_\perp$ is the speed in the plane perpendicular to z, and $\mathcal{M} \equiv \rho \sin\phi_v$ is the moment arm or "reduced" angular momentum. Specifically, ϕ_v is the azimuthal angle between the velocity $\mathbf{v}_\perp$ and $\hat{\boldsymbol{\rho}}$ [i.e., $\phi_v = \arccos(\hat{\boldsymbol{\rho}} \cdot \hat{\mathbf{v}}_\perp)$]. Therefore the quantity $v_\perp \mathcal{M}$ is the angular momentum about the z axis per unit mass.

The justification for these variables $(\rho, z, v_z, v_\perp, \mathcal{M})$ can be found in Ref. [8]. In summary, the velocity vector is split into v_z and $v_\perp$ so that the "ballistic motion" can be decoupled into two moves (see below). The choice to use $\mathcal{M}$ is partly because it is a conserved quantity during the ballistic motion (in the case of zero electric field). More importantly, however, a mesh in (v_ρ, v_ϕ) leads to unacceptable numerical diffusion. As electrons move radially outward in ρ in the absence of an electric field, the angle ϕ_v decreases (where ϕ_v is defined to be zero for an electron moving purely radially outwards). Electrons in the smallest ϕ_v cell at one radius should be placed in a smaller ϕ_v cell at the next radius they go to. On a uniform ϕ_v mesh this is impossible, unless there is a cell at $\phi_v = 0$. A cell at $\phi_v = 0$ will then trap electrons at $\phi_v = 0$ if they bounce off the outer radial wall and move to smaller radii. In either case, electrons are "pumped" towards or away from $\phi_v = 0$. Numerical diffusion then becomes a severe problem.

The way to avoid this systematic inaccuracy is to choose a mesh on which cells from one radius are mapped exactly onto cells at all other radii (at least when the electric field is zero). This essentially means using $\mathcal{M}$ to define the mesh. The $\mathcal{M}$ mesh has two distinct parts, one for electrons with negative radial velocities (inward going) and one with positive radial velocities (outward going). Figure 8 is an illustration of the mesh in the $(\rho, \mathcal{M})$ plane. The halves of the mesh share a single $\mathcal{M}$ cell at the smallest radius which can be reached by particles with that $\mathcal{M}$. The innermost cell is labeled a_0 in Fig. 8, and it includes ρ values from 0 to ρ_1 and $\mathcal{M}$ running from 0 to ρ_1 (since $\mathcal{M}_{max} = \rho_1 \sin\phi_{max}$). At the second radial cell, extending from ρ_1 to ρ_2, we have three $\mathcal{M}$ cells, one inward going and one outward going from $\mathcal{M} = 0$ to $\mathcal{M} = \rho_1$, and a third split cell from $\mathcal{M} = \rho_1$ to $\mathcal{M} = \rho_2$. This continues all the way to the last radial cell, extending from $\rho_{\mathcal{N}-1}$ to $\rho_{\mathcal{N}}$ which has $2\mathcal{N} - 1$ cells in $\mathcal{M}$.

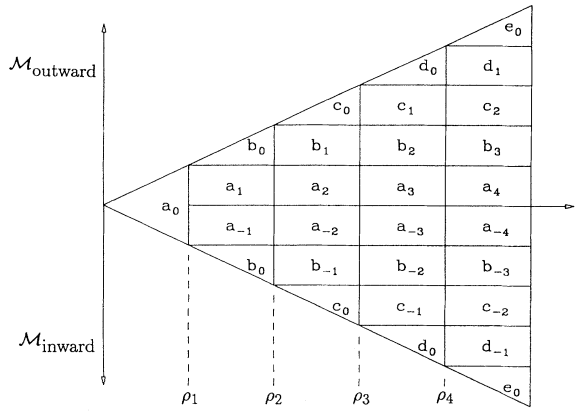

FIG. 8. Schematic of the $(\mathcal{M}, \rho)$ mesh used in the CS.

For an ICP discharge, or for any discharge which has an azimuthal electric field, the full range of ϕ_v (from 0 to 2π) must be represented. Therefore, Fig. 8 only represents half of the mesh, say for electrons with a positive angular momentum about the z axis. There is an identical mesh for electrons with a negative angular momentum about the z axis.

2. The ballistic and collisional propagators

In this section, we first describe the way in which the collisionless motion (or the ballistic move) of the electrons is implemented numerically. The collisional motion is essentially identical to that described in Ref. [8]; however, two minor changes will be discussed.

In this model, there are two separate motions each in a space coordinate and the corresponding velocity, which for conciseness we describe as motion in the spatial coordinates z and ρ. The first is the motion in the z direction and the second is the motion in the plane perpendicular to z. The motion in z is described in Refs. [6] and [7]. The motion perpendicular to the z axis is described in Ref. [8]. However, in Ref. [8], it was assumed that there was only a radial electric field E_ρ. In an ICP discharge, there is an azimuthal electric field E_θ, which sustains the discharge. We will now describe the extensions of this ballistic move to include the effects of the azimuthal electric field.

As described in Ref. [8], the ballistic move is based on the conservation of phase space volume (density). A given initial cell indexed by (i, j, k, l) has "mean" values $\overline{\rho}_i$, $\overline{v}_{\perp,j}$, $\overline{\mathcal{M}}_k$, and $\overline{v}_{z,l}$ and "boundary" values at ρ_{i-1}, ρ_i, $v_{\perp,j-1}$, $v_{\perp,j}$, $\mathcal{M}_{k-1}$, $\mathcal{M}_k$, $v_{z,l-1}$, and $v_{z,l}$, where $\overline{\rho}_i = (\rho_i + \rho_{i-1})/2$, etc., except for $\overline{\mathcal{M}}_k$. The particle density in a cell is assumed to be independent of the ϕ_v. This means that $\overline{\mathcal{M}}_k \equiv \int_{\Delta\phi_v} \mathcal{M} d\phi_v / \Delta\phi_v$, where $\Delta\phi_v$ is the range of ϕ_v in the cell.

In Ref. [8], it was shown that the initial cell "swept out" a phase space volume, during a time step Δt, given by

$$\Delta\eta_{i,j,k,l} = \pi(\mathcal{M}_k - \mathcal{M}_{k-1})\overline{\overline{v}_{\perp,j}}(v_{\perp,j}^2 - v_{\perp,j-1}^2) \times (v_{z,l} - v_{z,l-1})\Delta t, \tag{A1}$$

where $\overline{\overline{v}_{\perp,j}} = \overline{v}_{\perp,j}$ if there is no electric field. This "swept-out" phase space is then used to compute where the electrons move in the radial direction.

When a radial and azimuthal electric field is included, we then use the equation of motion for $v_\perp$:

$$\dot{v}_\perp = \frac{-e}{m}\left[\pm E_\rho(\rho,z)\left(1 - \mathcal{M}^2/\rho^2\right)^{1/2} + E_\theta(\rho,z)\mathcal{M}/\rho\right]. \tag{A2}$$

The minus sign is used for inward going electrons and m is the electron mass. During the computation of $\Delta\eta$, $\overline{\overline{v}_{\perp,j}}$ is approximated as

$$\overline{\overline{v}_{\perp,j}} = \overline{v}_{\perp,j} - \frac{e}{2m}\left[\mp E_\rho(\rho,z)(1 - \overline{\mathcal{M}}_k^2/\overline{\rho}_i^2)^{1/2} + E_\theta(\rho,z)\overline{\mathcal{M}}_k/\overline{\rho}_i\right]\Delta t. \tag{A3}$$

The error in this approximation decreases with decreasing mesh size; the error vanishes for an infinitesimal mesh size. The above equation defines a time average $v_\perp$ during Δt. For an initial cell, the volume of phase space "swept out" is computed for each radial boundary by using E_ρ and E_θ at each boundary. This allows the initial phase space volume to expand or contract in the radial direction.

Once the spatial distribution is found, conservation of energy is used to update the distribution in $v_\perp$. Suppose some of the electrons from the initial cell with mean radius $\overline{\rho}_i$ and mean velocity $\overline{v}_{\perp,j}$ are distributed to a final spatial cell with mean radius $\overline{\rho}_m$. These electrons should, by conservation of energy, have a moved perpendicular velocity $v'_\perp$ given by

$$v'_\perp = \left(\overline{v}_{\perp,k}^2 + \frac{2e}{m}[\Phi(\overline{\rho}_m,z) - \Phi(\overline{\rho}_i,z)] + \frac{2}{m}W\right)^{1/2} \tag{A4}$$

where $\Phi(\rho,z)$ is the electrostatic potential and W is the work done by the azimuthal electric field. We calculate W by the energy theorem

$$\dot{W} = -eE_\theta v_\perp \mathcal{M}/\rho. \tag{A5}$$

The computation of W is approximated as

$$W = -e\overline{E}_\theta\left(\overline{v_\perp\mathcal{M}/\rho}\right)\Delta t \tag{A6}$$

where $\overline{E}_\theta$ is the average E_θ over the electron trajectory. If $\overline{E}_\theta$ is accelerating the electron, then we find

$$W = -e\overline{E}_\theta\Delta t\left[v_{\perp,j}\mathcal{M}_k - \frac{e}{2m}\overline{\rho}\overline{E}_\theta\Delta t\right]/\overline{\rho}_m \tag{A7}$$

where $\overline{\rho}$ is the average ρ over the electron trajectory. However, if $\overline{E}_\theta$ is decelerating the electrons, then W is given by

$$W = \begin{cases} -\frac{1}{2}mv_{\perp,j}^2\mathcal{M}_k^2/\overline{\rho}_m^2 + [e\overline{E}_\theta(\Delta t - \beta)]^2\frac{\overline{\rho}}{2m\overline{\rho}_m} & \text{for } \beta < \Delta t \\ -e\overline{E}_\theta\Delta t[v_{\perp,j}\mathcal{M}_k - \frac{e}{2m}\overline{\rho}\overline{E}_\theta\Delta t]/\overline{\rho}_m & \text{for } \beta > \Delta t, \end{cases} \tag{A8}$$

where $\beta = 2mv_{\perp,j}\mathcal{M}_k/(e\overline{\rho}|\overline{E}_\theta|)$. The error in this approximation decreases with decreasing mesh size also.

Typically $v'_\perp$ [Eq. (A4)] does not correspond exactly to the mean $v_\perp$ in a cell on the mesh, in which case the electrons are shared between the two neighboring $v_\perp$ cells in such a way that kinetic energy (in the azimuthal plane) is conserved. If a final radial spatial cell is energetically forbidden, the electrons retrace their trajectory to the previous radial cell, reversing the sign of their radial velocity.

Once ρ and $v_\perp$ distributions are updated, the $\mathcal{M}$ distribution must be updated. The electrons distributed to a final cell with mean radius $\overline{\rho}_m$ and a final speed $v'_\perp$ have a range of final $\mathcal{M}'$, from $\mathcal{M}'_-$ to $\mathcal{M}'_+$. This range is found from the initial range of $\mathcal{M}$ (i.e., $\mathcal{M}_{k-1}$ through $\mathcal{M}_k$) and the average torque over the electron trajectory:

$$\mathcal{M}'_\mp = \left(\mathcal{M}_q v_{\perp,j} - \frac{e}{m}\overline{\rho}\overline{E}_\theta\Delta t\right)/v'_\perp, \tag{A9}$$

where q is equal to $k-1$ or k. From this range of $\mathcal{M}'$, a range of $\mathcal{M}$ cells is found and the electrons are distributed uniformly in ϕ_v in these $\mathcal{M}$ cells. If the torque equation cannot be satisfied or the range of $\mathcal{M}$ shrinks to zero, then the electrons retrace their trajectory to the previous radial cell, reversing the sign of their radial velocity.

If a magnetic field in the z direction is added, the algorithm is slightly adjusted as follows. This component of the magnetic field, B_z, produces a rotation of $v_\perp$ about the z axis by the angle $\frac{-e}{m}B_z\Delta t$ but does not change the magnitude of $v_\perp$. As the phase space volume is swept out, we check to see if $\overline{B}_z$ (the average B_z over the trajectory) has reversed the radial velocity. If so, that radial cell is declared "forbidden" and the electrons reverse their radial velocity. Otherwise the final spatial distribution is found as above. The only difference is that the final $\mathcal{M}$'s must be adjusted (rotated). A magnetic field in the radial direction, B_r, would mix the components of v_z and $v_\perp$. As such, this Lorentz force term would be on equal footing with the E_θ term.

Due to the finite cell size of our spatial grid and total energy conservation in the ballistic move, the very lowest-energy particles can be artifically "trapped" in certain cells. Previously we have developed an algorithm to eliminate this problem by estimating the steady-state momentum in a cell so that the flux out of a spatial cell is correct.

For particles with identically zero kinetic energy, the scheme for correcting the momentum has been further developed. A particle with zero kinetic energy will be accelerated by the fields present. As the particle is accelerated, the collision frequency is given by $N\sigma(at)at$, where a is the acceleration, N is neutral density, t is the time, and σ is the total cross section. For now we assume

$\sigma(at) = \text{const.}$

The probability of collision during a time t is given by

$$P = 1 - \exp(-N\sigma a t^2) \tag{A10}$$

which can be inverted to give $t(P)$:

$$t(P) = [-\ln(1-P)/(N\sigma a)]^{1/2}. \tag{A11}$$

The average t, $\langle t \rangle$, before a collision (i.e., the average over the above distribution from P=0 to 1) is given by

$$\langle t \rangle = \sqrt{\pi/(N\sigma a)}/2. \tag{A12}$$

For each spatial cell on the mesh, electrostatic fields are specified and the acceleration a can be computed and therefore $\langle t \rangle$ for each spatial cell can be found.

To correct for the flux (or momentum) of the initially zero energy particles, the average velocity can be taken to be

$$\langle v \rangle = 0.5 a \langle t \rangle \tag{A13}$$

and thus a particle will move a distance

$$dx = \langle v \rangle \Delta t = 0.5 a \langle t \rangle \Delta t \tag{A14}$$

where Δt is the time step of the simulation.

Since σ, in general, is not constant, one can find an average σ given that the particle started at v=0 and finished with $v = a\langle t \rangle$. A simple iterative technique, if needed, can be used to find a better estimate of $\langle t \rangle$.

Before we end this section, we mention two minor revisions to the collisional propagators. The first concerns electron-electron Coulomb collisions and the second is for electron-neutral collisions.

Reference [7] described how electron-electron Coulomb collisions were implemented numerically. Essentially, the EDF is fitted to a finite number of Maxwellian distributions and then analytic expressions give the energy transfer rate between pairs of Maxwellian distribution functions. An algorithm was described which conserved particle number and energy exactly on the numerical mesh. We simply stress that for the scheme to work properly the fitted distributions must accurately represent the low-energy part of the EDF.

The other minor revision concerns electron-neutral collisions. As described in Ref. [8], the fraction of electrons scattering during a time step is given by

$$N_{\text{scatt}}/N_{\text{cell}} = \sigma_k \left(\overline{v}_{z,i}^2 + \overline{v}_{\perp,j}^2 + 3k_B T_g/M\right)^{1/2} N \Delta t, \tag{A15}$$

where N_{cell} is the number of electrons in the phase space cell, σ_k is the cross section for the kth collision, T_g and M are the neutral temperature and mass, respectively, k_B is Boltzmann's constant, and N is the neutral density. The final velocity of these scattered electrons is

$$v' = \left(\overline{v}_{z,i}^2 + \overline{v}_{\perp,j}^2 + \frac{2\Delta\tau_k}{m}\right)^{1/2} \tag{A16}$$

where $\Delta\tau_k$ is the change in energy due to collision k. Isotropic redistribution is accomplished by putting a fraction $(v_{z,p} - v_{z,p-1})/v'$ of the scattered electrons into the pth cell for all $|v_{z,p}| < v'$. The corresponding $v_\perp$ cell(s) are at

$$v_\perp' = [(v')^2 - \overline{v}_{z,p}^2]^{1/2}. \tag{A17}$$

Usually the absence of a $v_\perp$ cell at this precise $v_\perp'$ requires splitting the electrons between two adjacent cells in a fashion which conserves energy.

The revision is concerned with Eq. (A17). Instead, we find two $v_\perp$'s by

$$v_{\perp,\pm}' = [(v')^2 - \overline{v}_{z,q}^2]^{1/2} \tag{A18}$$

where q is equal to $p-1$ or p. These $v_{\perp,\pm}'$'s give a range of $v_\perp$ cells where the scattered electrons are redistributed in such a way that the correct fraction goes to the $v_{z,p}$ cell and energy is conserved.

3. Algorithm of the CS in an ICP

In this section, we describe the algorithm of the CS for modeling electrons in an ICP discharge. The algorithm typically consists of three modules: ballistic move in the "z direction," ballistic move in the "direction perpendicular to z," and collisions. Typically, an electrostatic potential $\Phi(\rho, z)$ and inductive field $E_\theta(\rho, z, t)$ are input to the CS. During a typical time step, first the ballistic moves are done (the order of calling is alternated between successive time steps). Then, from the atomic cross sections, a collision time is found. If a preset small fraction (typically 1/5) of the collision time has elapsed since the last time the collision routine was called, the electron-neutral collisions are executed. Then, using a similar technique, it is decided if electron-electron Coulomb collisions should be called (see Ref. [8]). The azimuthal electric field is then advanced in time (including any capacitive fields, if present) and the time step is repeated.

The typical time step in the ICP simulation is $\sim 1/50$ of the rf period. This rather long time step is possible since this is not a self-consistent calculation (that is, Poisson's equation is not solved), though this time step is small enough to resolve the sinusoidal fields. In the simulations reported here, the electrons are not affected by the inductive magnetic fields. While these effects may become significant in an ICP, at the pressures and frequencies studied here they are not believed to strongly affect the electron kinetics.

[1] M.A. Lieberman and A.J. Lichtenberg, *Principles of Plasma Discharges and Materials Processing* (John Wiley & Sons, Inc., New York, 1994).
[2] V.I. Kolobov and V.A. Godyak, IEEE Trans. Plasma Sci. **23**, 503 (1995); L.D. Tsendin, Plasma Sources Sci. Technol. **4**, 200 (1995).
[3] J.P. Boeuf and L.C. Pitchford, IEEE Trans. Plasma Sci. **19**, 286 (1991); A.M. Popov, A.T. Rakhimov, and T.V. Rakhimova, Plasma Phys. Rep. **19**, 651 (1993).
[4] C.K. Birdsall and A.B. Langdon, *Plasma Physics via Computer Simulation* (McGraw-Hill, New York, 1985); R.W. Hockney and J.W. Eastwood, *Computer Simulation Using Particles* (IOP Publishing, Bristol, 1988); C.K. Birdsall, IEEE Trans. Plasma Sci. **19**, 65 (1991).
[5] W.N.G. Hitchon, D.J. Koch, and J.B. Adams, J. Comput. Phys. **83**, 79 (1989); H. Sugawara, Y. Sakai and H. Tagashira, J. Phys. D **25**, 1483 (1992); J. Bretagne, G. Gousset, and T. Simko, *ibid.* **27**, 1866 (1994).
[6] G.J. Parker, W.N.G. Hitchon, and J.E. Lawler, J. Comput. Phys. **106**, 147 (1993); W.N.G. Hitchon, G.J. Parker, and J.E. Lawler, IEEE Trans. Plasma Sci. **21**, 228 (1993).
[7] W.N.G. Hitchon, G.J. Parker, and J.E. Lawler, IEEE Trans. Plasma Sci. **22**, 267 (1994).
[8] G.J. Parker, W.N.G. Hitchon and J.E. Lawler, Phys. Rev. E **50**, 3210 (1994).
[9] V.I. Kolobov, D.F. Beale, L.J. Mahoney, and A.E. Wendt, Appl. Phys. Lett. **65**, 537 (1994).
[10] U. Kortshagen and L.D. Tsendin, Appl. Phys. Lett. **65**, 1355 (1994).
[11] V.I. Kolobov and W.N.G. Hitchon, Phys. Rev. E **52**, 972 (1995).
[12] U. Kortshagen, I. Pukropski, and L.D. Tsendin, Phys. Rev. E **51**, 6063 (1995).
[13] P.L.G. Ventzek, R.J. Hoekstra, and M.J. Kushner, J. Vac. Sci. Technol. B **12**, 461 (1994).
[14] V.A. Godyak, R.B. Piejak, and B.M. Alexandrovich, Plasma Phys. Sci. Technol. **3**, 169 (1994).
[15] M.M. Turner, Phys. Rev. Lett. **71**, 1844 (1993).
[16] V. Vahedi, M.A. Lieberman, G. DiPeso, T.D. Rognlien, and D. Hewett, J. Appl. Phys. **78**, 1446 (1995).
[17] J.W. Eastwood, Comput. Phys. Commun. **43**, 89 (1986); **44**, 73 (1987).
[18] T.J. Sommerer, W.N.G. Hitchon. R.E.P. Harvey, and J.E. Lawler, Phys. Rev. A **43**, 4452 (1991).
[19] E.V. Karoulina and Y.A. Lebedev, J. Phys. D **21**, 411 (1988).
[20] V.A. Godyak and R.B. Piejak, Appl. Phys. Lett. **63**, 3137 (1993).
[21] L.J. Mahoney, A.E. Wendt, E. Barrios, C.J. Richards, and J.L. Shohet, J. Appl. Phys. **76**, 2041 (1994).
[22] V.I. Kolobov and L.D. Tsendin, Phys. Rev. A **21**, 411 (1992).
[23] G.J. Parker, W.N.G. Hitchon, and J.E. Lawler, Phys. Lett. A **174**, 308 (1993).